Perceptually Optimizing Color Look-up Tables

Johann Reinhard and Philipp Urban

***Abstract*— The quality of ICC profiles with embedded look-up tables (LUTs) depends on multiple factors: 1. the accuracy of the optical printer model, 2. the exploitation of the available gamut combined with the quality of the gamut mapping approach encoded in the B2A-LUTs (backwards LUTs) and 3. the tonal smoothness as well color accuracy of the backwards LUTs. It can be shown that optimizing the smoothness of the LUTs comes at the expense of color accuracy and requires gamut reduction because of internal tonal edges. We present a method to optimize backwards LUTs of existing ICC profiles w.r.t accuracy, smoothness, gamut exploitation and mapping, which can be extended beyond color, e.g. to joint color and translucency backward LUTs. The approach is based on a perceptual difference metric that is used to optimize the LUT's tonal smoothness constrained to preserve both the accuracy of and the relationship between colors.**

***Index Terms*— Digital printing, image quality, color, gamut mapping, table lookup, 3-dimensional printing.**

I. Introduction

COLOR look-up tables (CLUTs) are widely used by color management systems (such as by the International Color Consortium [1]) for cross-media color reproduction. They approximate and encode non-linear transformations between device-independent (e.g. CIELAB) and device-dependent (e.g. CMYK) spaces. In particular for printing applications they combine highly-nonlinear color gamut mapping and separation algorithms allowing an extremely fast evaluation of the joint transformation. As one of the key-factors affecting print quality, CLUTs were the topic of a large body of research in the past decades [2], [3], [4], [5], [6], to name a few.

In this work, we focus on CLUTs for reproducing given colors in printing, such as the B2A-CLUTs in ICC-printer-profiles, but also investigate color-related improvements of LUTs for appearance reproduction in which appearance correlates beyond color are considered, such as translucency [7], [8]. The latter tables exploit larger degrees-of-freedom of graphical 3D printing to reproduce appearance correlates beyond color. The color-related quality of all such CLUTs depends on multiple factors:

1) the accuracy of the optical printer model that predicts spectral or color values from tonal values,
2) the exploitation of the available color gamut combined with the quality of the gamut mapping approach,
3) the tonal smoothness as well color accuracy of the B2A-CLUTs that determine the tonal values for a color.

For printing systems with more than CMY colorants, more than one tonal combination can map to the same color or even to almost the same reflectance [9]. Such redundancies must be taken into account while computing the CLUT nodes because mapping neighboring node-colors to very different tonals may cause large color errors when interpolating between them. This results in structural artifacts of the simulated print (see Fig. 1). Smoothing the CLUT minimizes such artifacts but comes at the expense of reducing color accuracy.

CLUT discontinuities can be also the result of sharp edges of gamut boundaries in combination with distinct gamut mapping algorithms, which may cause nearby out-of-gamut colors to be mapped to distant in-gamut-colors reproducible only with very different tonal values [10]. But even if the gamut mapping transform is smooth, nearby points on the gamut boundary might be reproducible only by very different tonal values. This is the case for printing systems with more than three colorants since an N-dimensional tonal value hypercube ($N > 3$) is mapped to a three-dimensional color space and nearby points on the gamut boundary may correspond to different tonal hypercube facets as illustrated in Fig. 2 [11] and [12]. In this case exploiting the full printer gamut with a smooth CLUT is impossible. Creating a smooth CLUT for such printers is only possible by removing parts of the gamut to ensure that any path on the resulting gamut boundary can be reproduced by a smooth transition in tonal value space.

Methods have been proposed to optimize CLUTs w.r.t to single or multiple criteria. Morovič et al. proposed an accuracy preserving smoothing along lightness [13] that does not correct gamut-mapping-induced discontinuities. Bhachech et al. extrapolated gamut boundary vertices to avoid gamut-mapping-induced CLUT discontinuities at the gamut boundary [14] but have not optimized for overall smoothness of the CLUT. To our knowledge no approach exists that optimizes a CLUT w.r.t. to all criteria, i.e. color accuracy, smoothness and gamut exploitation.

Manuscript received 6 April 2022; revised 25 September 2022 and 3 November 2022; accepted 18 November 2022. Date of publication 15 December 2022; date of current version 27 December 2022. This work was supported by the German Federal Ministry for Economic Affairs and Climate Action as AIF IGF Project FarbMod3D under Grant 20852 N/2. The associate editor coordinating the review of this manuscript and approving it for publication was Dr. Daniel L. Lau. *(Corresponding author: Johann Reinhard.)*

Johann Reinhard is with the Fraunhofer Institute for Computer Graphic Research IGD, 64283 Darmstadt, Germany, and also with the Department of Computer Science, Technische Universität Darmstadt, 64283 Darmstadt, Germany (e-mail: johann.reinhard@igd.fraunhofer.de).

Philipp Urban is with the Fraunhofer Institute for Computer Graphic Research IGD, 64283 Darmstadt, Germany, and also with the Department of Computer Science, Norwegian University of Science and Technology, 2815 Gjøvik, Norway (e-mail: philipp.urban@igd.fraunhofer.de).

This article has supplementary downloadable material available at https://doi.org/10.1109/TIP.2022.3228498, provided by the authors.

Digital Object Identifier 10.1109/TIP.2022.3228498

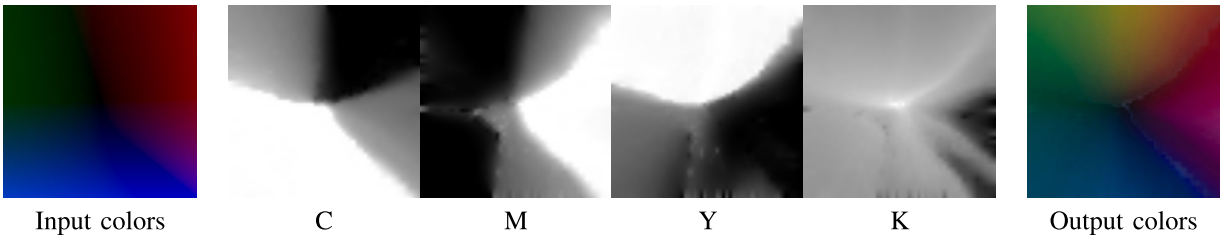

Fig. 1. Separation of the tonal values for reproducing an a*b*-plane and the resulting color prediction of the forward optical printer model for a multi-material 3D printer. Most colors are out of gamut and are gamut mapped. Edges in the tonal value images can result in structural artifacts in the color prediction, visible as whitish lines in the output. This is because similar node-colors of the CLUT are mapped to different tonal values and the multi-linear interpolation results in colors that are not similar to either node-color.

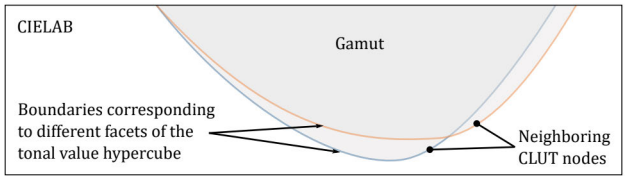

Fig. 2. Neighboring CLUT node colors located on the gamut boundary can only be reproduced with very different tonal values if they belong to different tonal value hypercube facets. In this case it is impossible to exploit the full gamut with a smooth CLUT.

A prerequisite of such an optimization is an objective function that incorporates a quality measure of the CLUT. This quality measure must judge color accuracy, gamut-mapping-induced distortion and structural artifacts caused by interpolation between color nodes with very different tonal values.

In this work we use an objective function based on iCID, a full reference color image quality metric particularly designed to judge gamut mapping distortions [15]. As an extension of the SSIM [16] on color images it is also computed on windows; given two color images A and B of equal size, $\mathbf{iCID}(A, B)$ computes internally for each pixel a dissimilarity score by evaluating a window $\mathbf{W}$ centered on the pixel.

iCID was also used to iteratively optimize the gamut mapping and achieved significantly better results in a psychophysical experiment compared to state-of-the-art gamut mapping algorithms [15]. A drawback of the iterative approach is its runtime performance, which prevents practical usage in various applications. This limitation is not given for optimizing existing CLUTs, since once created they can be used by performance-optimized color management modules in any existing workflow.

A CLUT encodes (in B2A tags of ICC profiles) a transformation $\mathbf{B}$: CIELAB $\mapsto$ Ω, where Ω is the tonal value space (e.g. CMYK). Such a CLUT provides tonal value combinations used by subsequent halftoning methods of the printing workflow to reproduce given CIELAB input. The transformation encoded in the CLUTs can be conceptually decomposed into $\mathbf{B} = \mathbf{p_{inv}} \circ \mathbf{g}$, where $\mathbf{g}$: CIELAB $\mapsto$ $\mathbf{p}(\Omega)$ is a gamut mapping transformation, $\mathbf{p}$: $\Omega \mapsto$ CIELAB is the optical forward printer model and $\mathbf{p_{inv}}$: CIELAB $\mapsto$ Ω is the backward printer model. Various gamut mapping transforms $\mathbf{g}$ can be used; e.g. for the relative colorimetric intent (B2A1) gamut clipping transforms are used and for the perceptual intent (B2A0) compression transforms are used [17]. Gamut clipping transforms possess the following property: $\forall x \in \mathbf{p}(\Omega) : \mathbf{g}(x) = x$. Since $\mathbf{p}$ is usually not injective, there are multiple backward models $\mathbf{p_{inv}}$ that are commonly computed by Gray Component Replacement (GCR) or Under Color Removal (UCR) strategies for selecting a distinct tonal combination from the set of combinations producing the same color. Note that $\forall x \in \mathbf{p}(\Omega) : \mathbf{p}(\mathbf{p_{inv}}(x)) = x$, but for a printer with more than CMY inks the following applies $\exists z \in \Omega : \mathbf{p_{inv}}(\mathbf{p}(z)) \neq z$.

In this paper we present two main contributions:

- An image difference metric based optimization of backwards LUTs of color profiles for full-color 3D printers.
- Extension of this optimization to create joint profiles of color and other appearance correlates, e.g. translucency.

In section V we show that our proposed algorithm significantly reduces artifacts in color-only and joint color and translucency printer profiles and creates much smoother reproductions of color gradients.

II. Overview

Symbols

Ω	Tonal value space.
$\mathbf{p}$	Optical printer forward model: $\Omega \mapsto$ CIELAB.
$\mathbf{B}$	Transform of B2A backward CLUT: CIELAB $\mapsto \Omega$.
LAB	Discrete sampled CIELAB color space.
$\mathbf{G_{LAB}}$	B2A CLUT grid points' position in CIELAB space.
$\mathbf{G}_\Omega$	Tonal values at the grid points.
$\mathbf{B}[x, z]$	$\mathbf{B}$ with tonal value at position $x \in \mathbf{G_{LAB}}$ replaced by $z \in \Omega$.
$\mathbf{B}^*$	Optimized Transform.
iCID	iCID image difference metric.
CIELCh	Cylindrical coordinate representation of CIELAB with lightness L*, chroma C*, and hue h predictors.
$\mathbf{q}$, $\mathbf{q}^{-1}$	Color space transformation CIELAB $\mapsto$ CIELCh, its inverse.
$\mathbf{r}$, $\mathbf{r}^{-1}$	Hue linearized mapping CIELAB $\mapsto$ CIELAB, its inverse.
$\mathcal{R}$	Set of reference images.

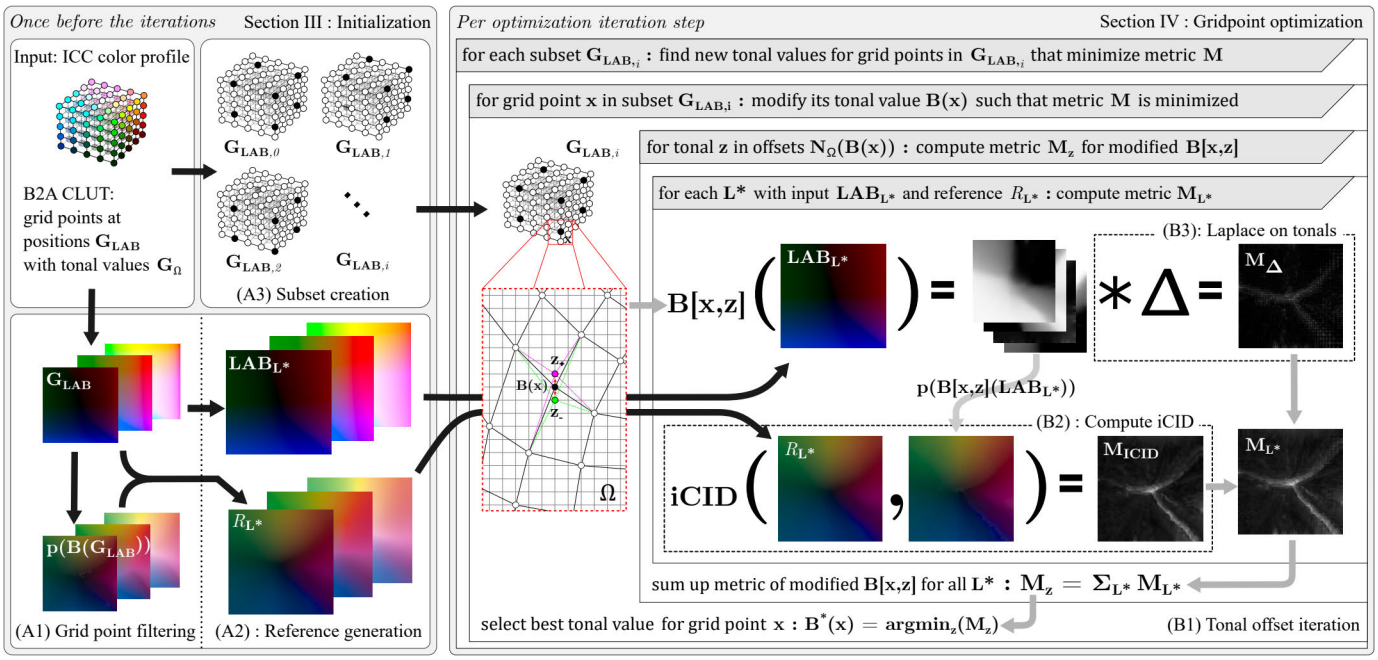

Fig. 3. Simplified overview of the iCID optimization. First we initialize the reference images R_{L^*} and separate the grid points into subsets $\mathbf{G_{LAB},}_i$. Then we optimize the grid points by repeating the following procedure for a fixed number of times: We sequentially iterate over all subsets $\mathbf{G_{LAB},}_i$ and for each grid point $x \in \mathbf{G_{LAB},}_i$ we search a new tonal value z. Based on its current tonal value $\mathbf{B}(x)$ we consider a set of alternative tonal values and modify the transform $\mathbf{B}[x, z]$. For each of these modified $\mathbf{B}[x, z]$ we compute the metric $\mathbf{M}$ using the input $\mathbf{LAB}_{L^*}$ and corresponding references R_{L^*}. The tonal value z that produces the smallest metric value becomes $\mathbf{B}(x)$. Note that the grid points in a subset $\mathbf{G_{LAB},}_i$ can be optimized in parallel, then the metric is only evaluated in the partition $P[x]$ of each grid point $x \in \mathbf{G_{LAB},}_i$.

Any real printer has a limited device gamut that can create the previously described color reproduction problems. The main idea is to use the **iCID** metric to quantify the difference between the desired colors and the colors reproduced by the printer, and then to iteratively modify the B2A CLUT that defines $\mathbf{B}$ to minimize the difference.

Naively we could find the optimal transformation $\mathbf{B}^*$ by

$$\mathbf{B}^* = \underset{\mathbf{B}}{\operatorname{argmin}} \sum_{L^*} \mathbf{iCID}(\mathbf{p}(\mathbf{B}(\mathbf{LAB}_{L^*})), \mathbf{LAB}_{L^*}) \qquad (1)$$

where $\mathbf{LAB}$ is a voxel grid discretizing the CIELAB color space, e.g. $\mathbf{LAB} = \{0, \ldots, 100\} \times \{-128, -127, \ldots, 127\}^2$, and we denote with $\mathbf{LAB}_{L^*} \subset \mathbf{LAB}, L^* \in \{0, \ldots, 100\}$ all voxels that have the same L^* value.

Using the entire CIELAB space as the input reduces structural artifacts and color differences for all colors and improves the previously mentioned color-related quality. However, using the entire CIELAB space as the desired output (which we denote as the ideal reference) results in large color differences to the reproduced colors by the printer because of its limited gamut. Minimizing the **iCID** metric then might introduce structural artifacts for the favor of reducing color differences. To avoid this we instead compare $\mathbf{p}(\mathbf{B}(\mathbf{LAB}_{L^*}))$ with a set of references that we derive from the initial backwards B2A CLUT which encodes the gamut and gamut mapping.

Our method is separated in two initialization steps and the iterative optimization itself as illustrated in Fig. 3. Using the B2A CLUT grid point's positions $\mathbf{G_{LAB}}$ and tonal values $\mathbf{G}_\Omega$ we first compute the references that define the optimal profile output, with respect to the limited gamut. Their creation consists of two parts (Fig. 3 A1 & A2) that are explained in detail in sections III-A.1 and III-A.2. The second initialization step splits the grid points into sets for an efficient iterative optimization (Fig. 3 A3) which is described in section III-B.

Then we repeatedly perform the optimization step of the transformation $\mathbf{B}$. For this we iterate over the sets and optimize for each grid point $x \in \mathbf{G_{LAB}}$ the tonal value (Fig. 3 B1). This changes the transformation $\mathbf{B}$, which is indicated by $\mathbf{B}[x, z]$ that represents the tonal value at grid point x being replaced by the tonal value $z \in \Omega$. We select the tonal value that minimizes a metric $\mathbf{M}$. As explained in section IV-A, $\mathbf{M}$ is the weighted sum of the iCID difference between $\mathbf{p}(\mathbf{B}(\mathbf{LAB}))$ and the references (Fig. 3 B2) and a Laplacian on the tonal value output $\mathbf{B}(\mathbf{LAB})$ (Fig. 3 B3). More details of the iterative algorithm are presented in IV-B. Once all grid points have been optimized once, the procedure either is repeated or terminates.

III. Initialization

We first extract from an ICC profile the B2A-CLUT, which defines the $\mathbf{B}$ transformation for the entire CIELAB color space by multi-linear interpolation, and A2B1-CLUT, which encodes the forward printer model $\mathbf{p}$. We denote by $\mathbf{G_{LAB}} \subset \mathbf{LAB}$ the grid point positions of the B2A-CLUT and by $\mathbf{G}_\Omega \subset \Omega$ the corresponding tonal values stored at these positions, i.e. $\mathbf{G}_\Omega = \mathbf{B}(\mathbf{G_{LAB}})$.

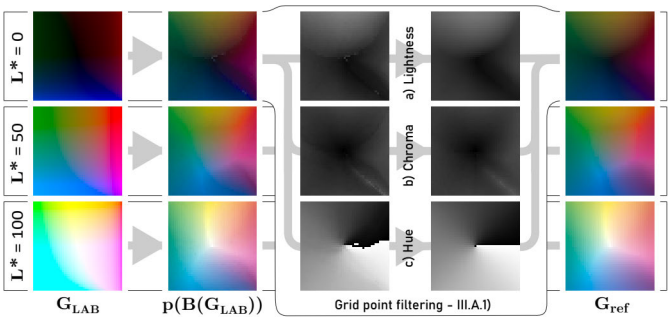

Fig. 4. Grid point filtering process: The discrete $\mathbf{G_{LAB}}$ grid points are mapped with $\mathbf{p}(\mathbf{B}(\mathbf{G_{LAB}})) = \mathbf{p}(\mathbf{G}_\Omega)$. The resulting 3-dimensional data structure is processed in the CIELCh color space where each channel is filtered separately. The output is combined and converted back to CIELAB forming the filtered reference colors $\mathbf{G}_{\mathrm{ref}}$.

Two initialization steps are necessary before the iterative optimization can start.

A. Reference Generation

As stated in (1) we could optimize $\mathbf{B}$ by comparing $\mathbf{p}(\mathbf{B}(\mathbf{LAB}_{\mathrm{L}^*}))$ with $\mathbf{LAB}_{\mathrm{L}^*}$ itself, but in practice the limited gamut results in significant color differences for out-of-gamut colors. This is a problem since the iCID optimization may favor structural artifacts to reduce large color errors, which we want to avoid in our CLUTs.

Therefore, instead of comparing with $\mathbf{LAB}_{\mathrm{L}^*}$ we compare with a set of reference images $\mathcal{R} = \{R_0, \cdots, R_{100}\}$ representing the optimal output of $\mathbf{p}(\mathbf{B}(\mathbf{LAB}_{\mathrm{L}^*}))$ for the different L* indices. Each reference R_{L^*} is a raster images that matches the corresponding $\mathbf{LAB}_{\mathrm{L}^*}$ in size. Thus we replace the optimization in (1) with

$$\mathbf{B}^* = \underset{\mathbf{B}}{\operatorname{argmin}} \sum_{\mathrm{L}^*} \mathbf{iCID}(\mathbf{p}(\mathbf{B}(\mathbf{LAB}_{\mathrm{L}^*})), R_{\mathrm{L}^*}) \tag{2}$$

The references $\mathcal{R}$ are derived such that they do not contain far out-of-gamut colors, yet they should represent the optimal output of the transformation. Inspired by heuristics used in various gamut mapping algorithms to reduce color, contrast and structural artifacts [18], we require the references to satisfy the following properties *a*) to *d*):

a) Monotone w.r.t. changes to lightness and smooth for constant lightness

b) Ideal chroma within the gamut, smooth chroma outside

c) Ideal hue everywhere

d) Preserve the profile's white point

Here and in the following any color $x \in$ CIELAB with a CIEDE2000 color difference of $\Delta E_{00}(x, \mathbf{p}(\mathbf{B}(x))) > 2.0$ is considered out-of-gamut.

1) Grid Point Filtering: To construct these references we use the grid points' tonal values $\mathbf{G}_\Omega = \mathbf{B}(\mathbf{G_{LAB}})$ and the forward model $\mathbf{p}$. The mapped colors $\mathbf{p}(\mathbf{G}_\Omega)$ of the grid points are generally similar to $\mathbf{G_{LAB}}$ within the gamut, but deviate from the ideal colors outside the gamut, which may create transitions that are not smooth. Therefore, we process or filter these colors, with the exception of the white point, to get reference colors $\mathbf{G}_{\mathrm{ref}} \in$ CIELAB that form the reference images $\mathcal{R}$. The steps are shown in Fig. 4. Using a hue-linearized CIELCh color space allows to process the predicted color attributes (lightness, chroma, and hue) independently with negligible cross-contamination between perceived attributes [19] in separate steps (neglecting perceptual phenomena such as the Helmholtz-Kohlrausch effect [20]).

Let $\mathbf{q}$: CIELAB $\mapsto$ CIELCh be the transformation to the CIELCh color space with the inverse $\mathbf{q}^{-1}$. Initialize $\mathbf{G_{LCh}} = \mathbf{q}(\mathbf{G_{LAB}}) \subset$ CIELCh as the ideal grid point colors in the CIELCh color space and $\mathbf{G}_{\mathrm{out}} = \mathbf{q}(\mathbf{p}(\mathbf{G}_\Omega)) \subset$ CIELCh as the corresponding mapped colors of the grid points' tonal values. The steps to achieve the desired properties *a*) to *d*) are

a) Lightness: For lightness we want to ensure monotonicity everywhere and smoothness outside of the gamut.

To achieve monotonicity we consider a column of colors $C_o \subset \mathbf{G}_{\mathrm{out}}$, where the corresponding $C_i \subset \mathbf{G_{LAB}}$ have the same a^* and b^*, and ensure, starting from the middle of the column going in both directions, that the lightness value is monotone by overwriting it with the previous lightness if not monotone. Afterward, each column C_o is monotone in L*.

To ensure smoothness we apply a conditional 2-dimensional box filter on points in the same a*-b*-plane that only replaces the lightness value if it is closer to the ideal lightness given by $c_i \in \mathbf{G_{LCh}}$. This ensures that values at the gamut boundary are not shifted towards values outside of the gamut.

These steps are repeated alternating a fixed number of times, until the desired smoothness is achieved, we chose in this case 10 times. A final monotonicity step at the end guarantees that the lightness of each column is monotone.

b) Chroma: We want to ensure that the chroma is ideal inside and smooth outside of the gamut. The processing is done in a hue linear space, e.g. according to [21]. For points inside the gamut we set the chroma to the chroma of the ideal color $c_i \in \mathbf{G_{LCh}}$. To ensure smoothness for colors outside of the gamut we apply a conditional 2-dimensional box filter in the a*-b*-planes, that only replaces the value if the average chroma is closer to the chroma of the ideal color $c_i \in \mathbf{G_{LCh}}$. This step is repeated n times to achieve the desired smoothness, where we use $n = 10$ in this work.

c) Hue: We want the hue to be ideal everywhere and use the hue of the ideal color $c_i \in \mathbf{G_{LCh}}$.

d) White point: The profile's white point is preserved by keeping it fixed at $\mathbf{p}(\mathbf{B}(x_{\mathbf{wp}})), x_{\mathbf{wp}} = (100, 0, 0) \in \mathbf{LAB}$.

We combine the results to T_R and compute the filtered grid points $\mathbf{G}_{\mathrm{ref}} = \mathbf{q}^{-1}(T_R)$ that satisfy the required properties $a), b), c)$ and $d)$ from above. They allow us to construct reference images without artifacts but also without any colors that are far away from the gamut.

2) Reference Image Generation: Each reference image $R_{\mathrm{L}^*} \in \mathrm{CIELAB}^{m \times m}$ of $\mathcal{R}$ is constructed from the filtered grid points $\mathbf{G}_{\mathrm{ref}}$ by trilinear interpolation. This leads to small errors in non-linear attributes, particularly the hue. Using $\mathbf{r}$: CIELAB $\mapsto$ CIELAB that maps to hue-linear corrected colors, for example based on Hung and Berns [21], and the inverse $\mathbf{r}^{-1}$, we process the references $\mathcal{R}$ via the following procedure that corrects the hue channel and also smooths the other channels for out-of-gamut colors:

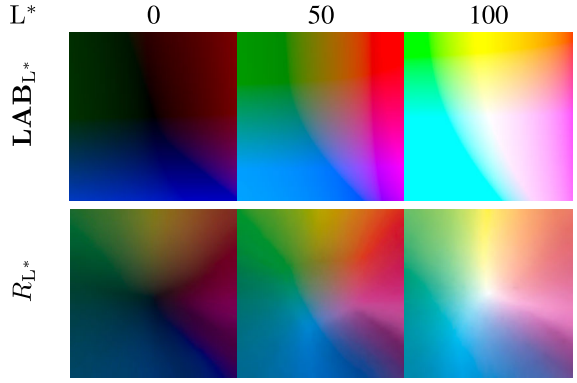

Fig. 5. Comparing the input $\mathbf{LAB}_{\mathrm{L}^*}$ images at the top, for $\mathrm{L}^* = 0$, 50,100 from left to right, with the corresponding reference images $R_{\mathrm{L}^*} \in \mathcal{R}$ generated from the filtered grid points $\mathbf{G}_{\mathrm{ref}}$ at the bottom shows, that the R_{L^*} contain no out-of-gamut colors but are also smooth without artifacts.

1) Set $R_{HL} := \mathbf{q}(\mathbf{r}(\mathcal{R})) \subset$ CIELCh
2) Iteratively smooth R_{HL} colors outside of gamut
   Lightness: 2D Box-Filter in C-h-plane
   Chroma: 3D Box-Filter
3) Set $I_{HL} := \mathbf{q}(\mathbf{r}(\mathbf{LAB})) \subset$ CIELCh
4) Set correct hue $R_{HL}(x)_h = I_{HL}(x)_h$
5) Finally $\mathcal{R} = \mathbf{r}^{-1}(\mathbf{q}^{-1}(R_{HL})) \subset$ CIELAB

Fig. 5 shows some of the resulting reference images R_{L^*} for $\mathrm{L}^* \in 0, 50, 100$, in comparison to the corresponding images $\mathbf{LAB}_{\mathrm{L}^*}$ of the discrete color space **LAB**. The supplemental includes additional images of $\mathcal{R}$, including separations of the lightness, chroma and hue channels, see Fig. 16 and 17.

B. Subset Separation and Partioning

The optimization can be parallelized with a similar way to phase group partitioning [22] given two observations:

1. Changes to a grid point's tonal value $\mathbf{G}_\Omega(x)$ alter only some colors in $\mathbf{p}(\mathbf{B}(\mathbf{LAB}))$. We define the partition $P[x] \subset \mathbf{LAB}$ of a grid point $x \in \mathbf{G}_{\mathbf{LAB}}$ to contain all elements in **LAB** that are enclosed in the volume spanned by the grid point's neighbors' positions, i.e. the positions of all grid points within a 3^3-window centered at x. Please note the correspondence between **LAB** and $\mathcal{R}$: pixels with the same index in $\mathbf{LAB}_{\mathrm{L}^*}$ and R_{L^*} correspond to each other; a partition $P[x]$ is defined for both.

2. Only pixels inside the 2-dimensional iCID window **W** affect the iCID value for a given pixel and the partition $P[x]$ represents all the pixels where the iCID is evaluated for x. Note that the iCID metric is evaluated on a*-b*-planes with constant L*, i.e. pixels in **W** might be outside $P[x]$ only w.r.t. their a*-b*-coordinates but never with their L*-coordinates.

Given these observations we separate the grid points into a minimal number n of disjoint sets $\mathbf{G}_{\mathbf{LAB},i}, i \in \{1, \cdots, n\}$ so that the grid points in each set satisfy the following condition:

$$\forall x_1, x_2 \in \mathbf{G}_{\mathbf{LAB},i}, x_1 \neq x_2,$$
$$\forall p \in P[x_2] : P[x_1] \cap \mathbf{W}(p) = \emptyset$$

The grid points in the same set $\mathbf{G}_{\mathbf{LAB},i}$ can then be optimized in parallel, since changes to their tonal values do not have any impact on each others iCID metric.

In Fig. 14 in the supplemental material we show how to exclude grid points based on this criterion exemplary in 2D.

IV. Optimization

After initialization, the tonal values in the table are iteratively optimized. One important constraint for this optimization is that the white point $w \in \mathbf{G}_{\mathbf{LAB}}$ must not be changed. In the following it is excluded from the sets, i.e. $\forall i : w \cap \mathbf{G}_{\mathbf{LAB},i} = \emptyset$.

A. Metric Definition

Let $\mathbf{L}(x)$ return the set of all unique L* positions in the partition $P[x]$ and define $P[x]_{\mathrm{L}^*}$ as the set of all positions in $P[x]$ with that L*, we define for a grid point position $x \in \mathbf{G}_{\mathbf{LAB}}$ an iCID based metric

$$\mathbf{M}_{\mathbf{iCID}}(\mathbf{B}, x) = \sum_{\mathrm{L}^* \in \mathbf{L}(x)} \frac{\mathbf{iCID}_{P[x]_{\mathrm{L}^*}}(\mathbf{p}(\mathbf{B}(\mathbf{LAB}_{\mathrm{L}^*})), R_{\mathrm{L}^*})}{|\mathbf{L}(x)|} \tag{3}$$

that is evaluated at all positions in the partition $P[x]$. We refer to [15] and (8) in the supplemental material for more details on the image difference metric $\mathbf{iCID}_A(X, Y)$. This metric allows selecting the optimal tonal values for a single grid point position x with respect to the iCID metric but does not consider the smoothness of the neighboring tonal values.

The latter is important for cases where the forward model **p** is not smooth, which would yield non-smooth tonal values for a maximally smooth output of **B** if just $\mathbf{M}_{\mathbf{iCID}}$ in (3) is used. To keep the transition between the tonal values smooth we define a tonal value space metric $\mathbf{M}_\Delta$ as

$$\mathbf{M}_\Delta(\mathbf{B}, x) = \frac{1}{|\mathbf{L}(x)|} \sum_{\mathrm{L}^* \in \mathbf{L}(x)} \Delta_{P[x]_{\mathrm{L}^*}}(\mathbf{B}(\mathbf{LAB}_{\mathrm{L}^*})) \tag{4}$$

where

$$\Delta_{P[x]_{\mathrm{L}^*}}(T) = \frac{1}{|P[x]_{\mathrm{L}^*}|} \sum_{p \in P[x]_{\mathrm{L}^*}} \frac{\|\nabla^2(T)(p)\|_1}{\dim(\Omega)} \tag{5}$$

with $\dim(\Omega)$ being the dimension of Ω and $\nabla^2(T)(p)$ being the second partial derivative of T evaluated at p. We approximate this by evaluating finite differences on the transformed reference images $\mathbf{B}(\mathbf{LAB}_{\mathrm{L}^*})$, i.e. just considering the a*-b*-plane.

We denote with **M** the combined metric that includes the iCID color term and the weighted Laplacian tonal term

$$\mathbf{M}(\mathbf{B}, x) = \mathbf{M}_{\mathbf{iCID}}(\mathbf{B}, x) + w\mathbf{M}_\Delta(\mathbf{B}, x) \tag{6}$$

with the weight w chosen such that the the Laplace term does not dominate the iCID term which is limited to [0, 1]. We then optimize this combined metric for each grid point

$$\mathbf{B}^*(x) = \underset{\mathbf{B}}{\operatorname{argmin}}\, \mathbf{M}(\mathbf{B}, x) \tag{7}$$

B. Iteration

We optimize the transformation **B** by minimizing the metric via variation of the tonal value entry of the B2A backwards CLUT for each grid point position. We denote by $\mathbf{B}[x, z]$ a locally modified **B** for which the tonal values at grid point position $x \in \mathbf{G}_{\mathbf{LAB}}$ are replaced by $z \in \Omega$.

Algorithm 1 Profile Optimization Step

OPTIMIZE($\mathbf{B}$)
  $\mathbf{B}^* \leftarrow \mathbf{B}$
  For each $i = 1, \ldots, n$
    For each $x \in \mathbf{G}_{\mathbf{LAB},i}$
      $N \leftarrow N_\Omega(\mathbf{B}^*(x))$
      $\mathbf{B}^*(x) \leftarrow \text{argmin}_{z \in N} \mathbf{M}(\mathbf{B}^*[x, z], x)$
  return $\mathbf{B}^*$

To select a new tonal value z for $\mathbf{B}(x) \in \mathbf{G}_\Omega$ we use the quantization of the tonal value space (usually 8 or 16 bits) and consider tonal values that differ one quantization step in one component, i.e. where $||z - \mathbf{B}(x)||_1 = 1$. Let $N_\Omega(z) : \Omega \mapsto \Omega^{(2 \cdot \dim(\Omega)+1)}$ return a set of the tonal value $z \in \Omega$ and all its direct L^1 neighbor tonal values.

Then the iterative optimization to update each grid point's tonal values $\mathbf{B}(x) \in \mathbf{G}_\Omega$ for all $x \in \mathbf{G}_{\mathbf{LAB}}$ of the B2A CLUT is performed by repeated execution of Algorithm 1.

Each iteration step optimizes all grid points of the B2A table one time with respect to the metric, with the exception of the white point whose values are fixed. Grid points that belong to the same set can be optimized in parallel, the sets are optimized sequentially for each step. Effectively to select the optimal tonal value for a grid point x we alter the tonal value, compute and average the metric over the partition $P[x]$ of the grid point and select the change with the minimal value.

Results using a fixed step size of 1 for variation of $\mathbf{B}(x)$ have shown that the optimization can get stuck in local minima. It is beneficial to vary the step size for the changes of $\mathbf{B}(x)$ along the tonal space axes, such that initially large and subsequently smaller changes allow the tonal values to gradually settle in a minimum. We choose to iterate through a set of step sizes based on a reversed Fibonacci series of fixed length, which is in detail explained in the supplemental material.

The optimization repeats this iteration step either until there is no change, i.e. until OPTIMIZE($\mathbf{B}$) $= \mathbf{B}$, or terminates after a fixed number of iterations. After the last iteration the optimized B2A CLUT of $\mathbf{B}^*$ is stored in the ICC profile.

C. Translucency

One interesting application for the iCID optimization is the construction of a joint color and translucency profile that characterizes a multi-material 3D printer employing a clear material in addition to the color materials. We define the color and tonal spaces similar to [7] and [23] using **CMYK**γ for the tonal space, with γ corresponding to the amount of clear material that replaces the white material, and CIELABα as the color space, with the α parameter according to Urban et al. [8]. For the α parameter, which ranges from $\alpha = 0.0$ fully transparent to $\alpha = 1.0$ fully opaque, we define T different discrete translucency levels t corresponding to the grid point position in the LUT, with translucency values $\alpha_t, t \in \{1, \cdots, T\}$ from fully opaque to fully transparent, i.e. $\alpha_1 = 1.0$ and $\alpha_T = 0.0$. Each of the translucency levels t is then optimized sequentially.

We define $\mathbf{p}_\gamma$: **CMYK**γ $\mapsto$ CIELABα as the mapping from the tonal space to the color-and-translucency space. There are different ways to determine such a mapping, for example Chen and Urban proposed deep-learning-based optical printer models to approximate $\mathbf{p}_\gamma$ with high accuracy requiring only a moderate number of printed and measured training samples [24]. We aim to compute the inverse B2A CLUT that maps CIELABα to **CMYK**γ by iteratively applying the previously described iCID optimization sequentially for incremental translucency levels t.

1) Initialization: From sampling the forwards model at the white point for different γ values, i.e. $\mathbf{p}_\gamma(z_{\mathbf{wp}}(\gamma))$ with $z_{\mathbf{wp}}(\gamma) = \{0, 0, 0, 0, \gamma\}$, we determine for each translucency level α_t the corresponding γ_t value where $\mathbf{p}_\gamma(z_{\mathbf{wp}}(\gamma_t))$ has an α component that best matches α_t. By definition $\gamma_0 = 0$ for the first translucency level α_1 and maximal for the last translucency level α_T. It is important to note that the transformation is therefore only accurate in α for the white point and likely has errors in the translucency reproduction anywhere else.

We denote by ${\mathbf{G}_\Omega}^t$ the grid points' tonal values for a particular translucency level α_t. Since the first translucency level α_1 represents the fully-opaque case with no transparent material we initialize ${\mathbf{G}_\Omega}^1 = \mathbf{G}_\Omega \times \{0\}$ to be the tonal values of the color-only table with $\gamma = 0$.

2) Iteration: The other tonal values ${\mathbf{G}_\Omega}^t, t \in \{2, \cdots, T\}$ are iteratively determined by the following approach. Each grid point of the next translucency level t is initialized with the values of the previous translucency level ${\mathbf{G}_\Omega}^{t-1}$ but with the value of γ set to the current γ_t.

To compute the metric the input colors **LAB** are augmented with the alpha value, i.e. $\mathbf{LAB}^t = \mathbf{LAB} \times \alpha_t$. Then we compute $\mathbf{p}_\gamma(\mathbf{B}^*(\mathbf{LAB}^t))$, from which we remove the alpha channel and compare it with the references $\mathcal{R}$ by evaluating the metric $\mathbf{M}$. We select again the change to the tonal value that minimizes $\mathbf{M}$, the γ component is not altered during the iteration.

V. Results

We applied the presented optimization on color profiles for two multi-material-jetting 3D printers, the Stratasys J750 and the Mimaki 3DUJ-553. Both printers can print with five color inks, CMYKW, a transparent material and a support material. The cyan material of the Mimaki printer is particularly dark, which results in a peculiarly shaped gamut that contains darker colors than the darkest color of the gray axis.

The ICC color profiles were generated with a proprietary profile creation software and contain a color-only B2A CLUT with 43^3 grid points and **CMYK** tonal values. They can also contain an embedded color-and-translucency profile utilizing the additional clear ink, with a 43^4 grid points B2A and **CMYK**γ tonal values. The tonal values are quantized as 16-bit unsigned integers.

Compared to the original iCID description [15] we slightly modified the metric by squaring the l_H hue-difference factor to better preserve the hue during the optimization. For the parameters of the optimization we use a kernel size of $k = 7$ for both the iCID window and Laplacian kernel. The weight for the Laplacian tonal term $\mathbf{M}_\Delta$ in the metric was $w = 0.005$,

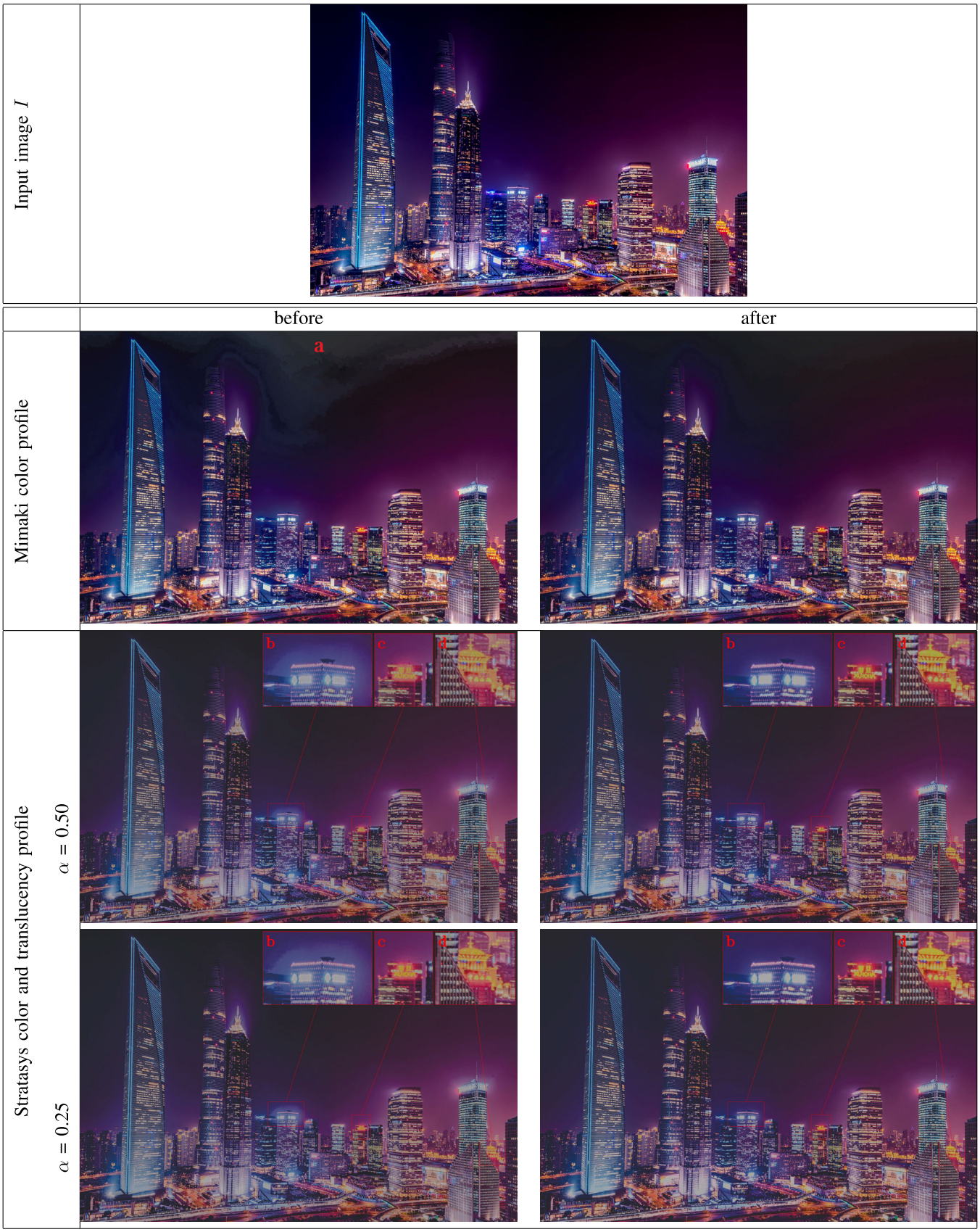

Fig. 6. Effect of the iCID optimization for both profiles on the simulation $\mathbf{p}(\mathbf{B}(I))$ of an input image I shown at the top. For the Mimaki color profile the severe artifact in the top of the image (a) is significantly reduced. For the Stratasys color and translucency profile the output is shown for two uniform RGBA alpha values. Note the reduced halo around the towers e.g. in the center with the blue signage (b), the better preserved red signage (c) on the right to it, as well as the generally more vibrant colors of the buildings in the right of the image (d); magnifications are shown in the top right. As described in V-B the gamut is particularly small and therefore challenging for $\alpha = 0.5$ due to lateral light transport. Here the optimization shows the biggest improvements.

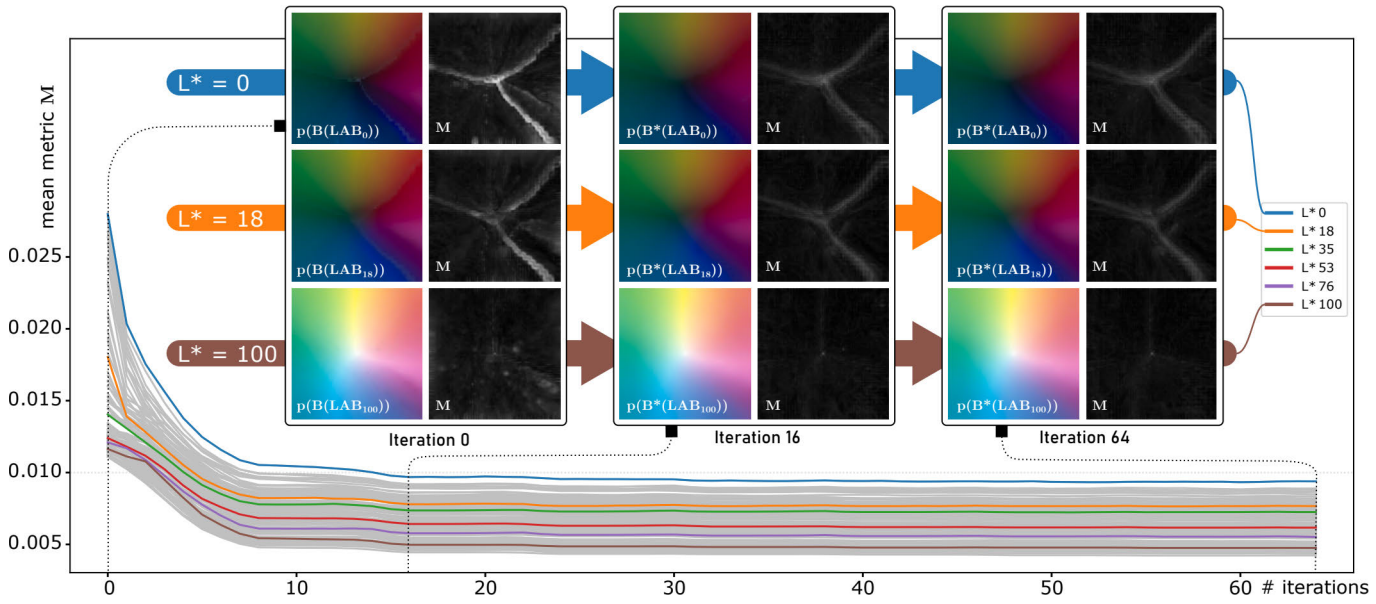

Fig. 7. Iterative reduction of the metric **M** for each L* image during the optimization of the Mimaki profile. Top visualizes exemplary results after 0, 16 and 64 iterations for images with L* = 0, 18 and 100; on the left $\mathbf{p}(\mathbf{B}(\mathbf{LAB}_{L^*}))$ the transformed image of the a*-b* plane at constant L* and on the right the corresponding metric **M** output when comparing to R_{L^*}. After a significant reduction of the average metric **M** in the first 8 iterations the curve flattens and after iteration 16 the metric remains almost constant. The images show that the output of the transformation $\mathbf{p}(\mathbf{B}^*(\mathbf{LAB}_{L^*}))$ becomes smoother and the structural artifacts are reduced or even removed.

we chose this value empirically such that the iCID color term $\mathbf{M_{iCID}}$ has a higher influence on the overall metric **M** than $\mathbf{M}_\Delta$. The image size m for the reference images is 256 pixels.

The algorithm was implemented in C++, with the iCID computation being accelerated using CUDA kernels. The LCMS2 color engine [25] was used to evaluate the **B** and **p** transforms embedded in the profiles and to modify the tonal values in the corresponding lookup tables. All experiments were run on a Windows 10 computer with an Intel Core i7 9700K, 64GB of RAM and a NVIDIA Geforce RTX 2080 Ti graphics card.

In Fig. 6 we highlight some of the improvements of the optimization in a real world example, the following sections provide a more quantitative analysis on the synthetic input and reference data.

A. Color Profile Optimization

To show that the proposed algorithm can reduce or remove artifacts we optimized an ICC color profile for the Mimaki 3DUJ-553 3D printer. The optimization iterated 8 times through the list {21, 13, 8, 5, 3, 2, 1, 1} of tonal step sizes, in total 64 iteration steps. We have empirically seen that more iterations did not further improve the output.

1) Metric Reduction: The left graph in Fig. 8 shows that the average metric for all colors is significantly reduced from 0.0150 to about 0.0067 after only 16 iterations A visual example of the results is given in Fig. 7 which also shows how the metric is evaluated and reduced in each $\mathbf{LAB}_{L^*}$ image of **LAB**. The initial color profile shows structural artifacts at the gamut edge in the transformed images $\mathbf{p}(\mathbf{B}(\mathbf{LAB}_{L^*}))$ before the first iteration, especially for dark colors with L* = 0 the white artifacts are quite visible. They are significantly reduced

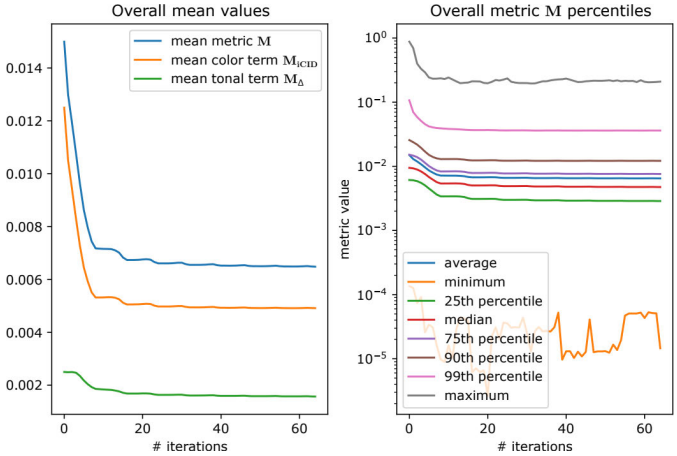

Fig. 8. Left graph: Effect of the optimization of the Mimaki profile on the overall metric **M** averaged over all pixels of the transformed $\mathbf{LAB}_{L^*}$ images. Note the staircase pattern that is a result of the varying step sizes for the tonal offsets. Also visible is that both the color term $\mathbf{M_{iCID}}$ and tonal term $\mathbf{M}_\Delta$ are reduced monotonically. Right graph: Also all percentiles and the maximum of the overall metric **M** are reduced.

in the optimized output $\mathbf{p}(\mathbf{B}^*(\mathbf{LAB}_{L^*}))$ after 16 iterations even though some errors still remain.

While the graphs show that additional iterations further reduce the average metric, which reaches a final value of 0.0065 after 64 iterations, the improvements between iteration 16 and 64 are only small and therefore hard to see in the transformed images or even the metric images. The right graph in Fig. 8 shows that also the maximal metric value and all evaluated percentiles are reduced in the optimization. Most of the curves follow an approximately exponential decay, after a limited number of iterations the improvements become only marginal yet measurable.

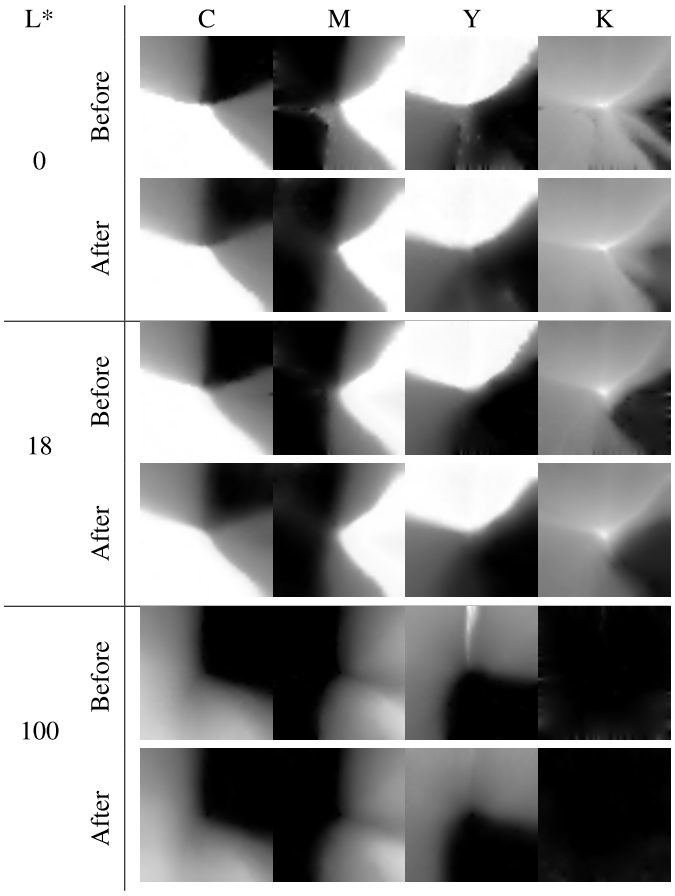

Fig. 9. CMYK tonal images of the Mimaki color profile for $L^* = 0$, 18 and 100 before $\mathbf{B}(\mathbf{LAB}_{L^*})$ (top rows) and after $\mathbf{B}^*(\mathbf{LAB}_{L^*})$ (bottom rows) the optimization. The smoothness is either preserved or visibly increased.

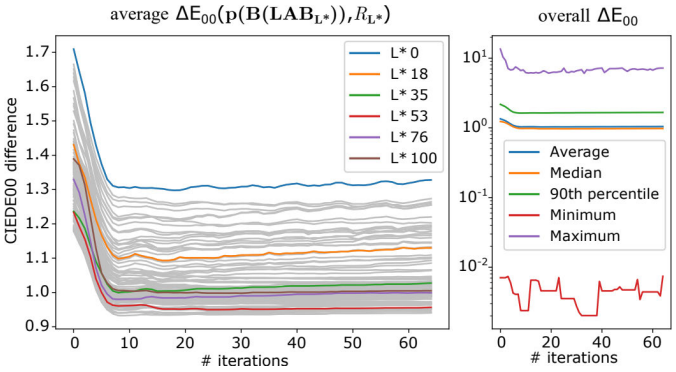

Fig. 10. CIEDE2000 difference between the references $\mathcal{R}$ and the simulation $\mathbf{p}(\mathbf{B}^*(\mathbf{LAB}))$ during the optimization. The left graph shows that on average the color difference is reduced in the first few iterations for each L^* image and then remains constant, however for some colors the optimization later on reduces structural artifacts at the expense of the color accuracy. The right graph shows that computed over all colors in **LAB** also the maximal, median and 90th percentile difference in comparison to the references is reduced.

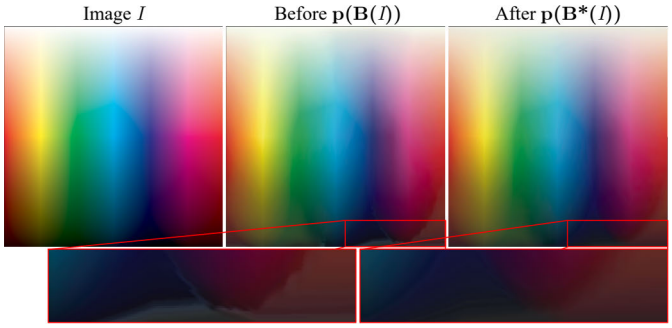

Fig. 11. Simulation of an image I that shows the surface of an CMYK printer's gamut visualized in sRGB (CMY varies left to right, K and total area coverage top to bottom). Left $\mathbf{p}(\mathbf{B}(I))$ before and on the right $\mathbf{p}(\mathbf{B}^*(I))$ after the optimization. Note the structural whitish artifacts on the bottom right of the left image, magnified below, that are reduced in the right image.

Concluding the plots show that the average metric was significantly reduced for all images $\mathbf{p}(\mathbf{B}^*(\mathbf{LAB}_{L^*}))$ in comparison to the references R_{L^*} thereby improving the profiles transformation to produce smoother yet still color accurate output. This smoothness is also visible in the transformed images shown in Fig. 7, the optimized profile especially improves the reproduction of color gradients. Structural artifacts are either removed or noticeably reduced, which is particularly apparent in the shown examples for $L^* = 0$ near the gray axis.

2) Tonal Term: The plot in Fig. 8 shows that the tonal Laplacian term $\mathbf{M}_\Delta$, which measures the smoothness in the tonal space, is also reduced during the optimization. This shows that the optimization is able to reduce both objective functions simultaneously. Looking at the tonal value images in Fig. 9 the output of the optimized transform $\mathbf{B}^*(\mathbf{LAB})$ is smoother compared to the initial $\mathbf{B}(\mathbf{LAB})$, especially for dark colors with small L^* values.

3) CIEDE2000: While the iCID metric contains a color term we want to validate that it is not dominated by the other terms such that the color accuracy is actually reduced during the optimization. To validate this we compare the transformed images $\mathbf{LAB}_{L^*}$ and the reference images R_{L^*} using a color difference formula, the CIEDE2000 color difference ΔE_{00}. We compute the pixel-wise color difference between the references $\mathcal{R}$ and the mapped colors $\mathbf{p}(\mathbf{B}^*(\mathbf{LAB}))$ for each L^* image separately but also overall and then statistically analyze the values, Fig. 10 shows the results.

We can see that the average CIEDE2000 color difference is reduced for all $\mathbf{LAB}_{L^*}$ images, also the overall average drops from 1.35 to around 1.04 and remains at this level for the remaining iterations. The median of the color difference follows the same trend, also the 90th percentile and maximal value are reduced and remain below the initial error. As the color difference is only one part of the metric it is not expected to be reduced in each iteration step, since other terms might dominate it, but the results show that the optimized profile is not only smoother but also exhibits a better color reproduction.

4) Runtime: Each optimization iteration takes about 80 seconds, the entire optimization with 64 iterations and the computation of the references takes about 90 minutes in total. Note that the optimization is an offline process and needs to be done only once.

a) Conclusion: The presented results show that our algorithm is able to improve both the color reproduction and smoothness of the **B** backwards model from the B2A table. For example structural artifacts are completely removed or strongly reduced in the optimized profile as shown in Fig. 11.

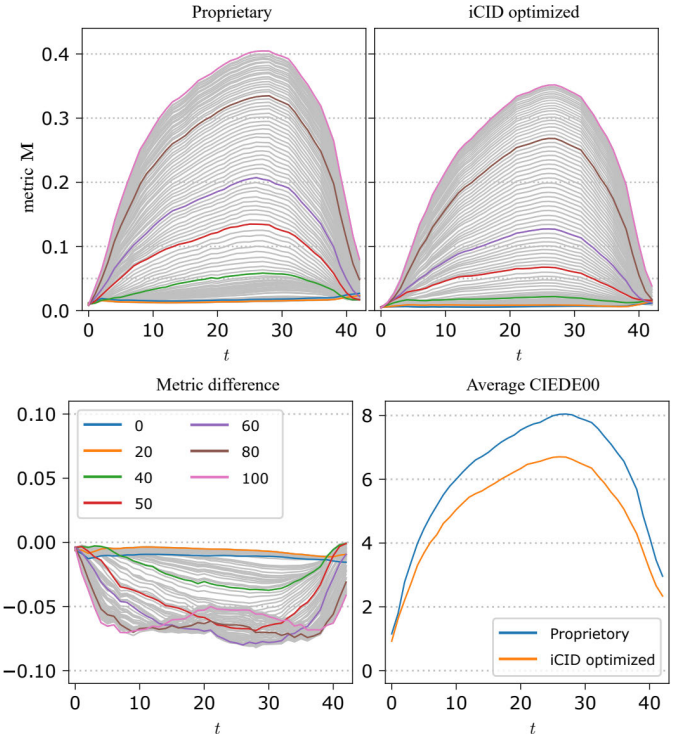

Fig. 12. Results of the iCID optimization for the Stratasys color and translucency profile. The upper plots show the average metric per L* slice for different translucency levels t when comparing the transformed input images to the references. Results for the profile created with the proprietary software on the left and for our algorithm on the right. As apparent from the graph in the lower left, that shows the difference between both results, the metric is generally smaller for the iCID optimized profile. Also the average CIEDE2000 color difference for each translucency level is smaller, shown in the lower right.

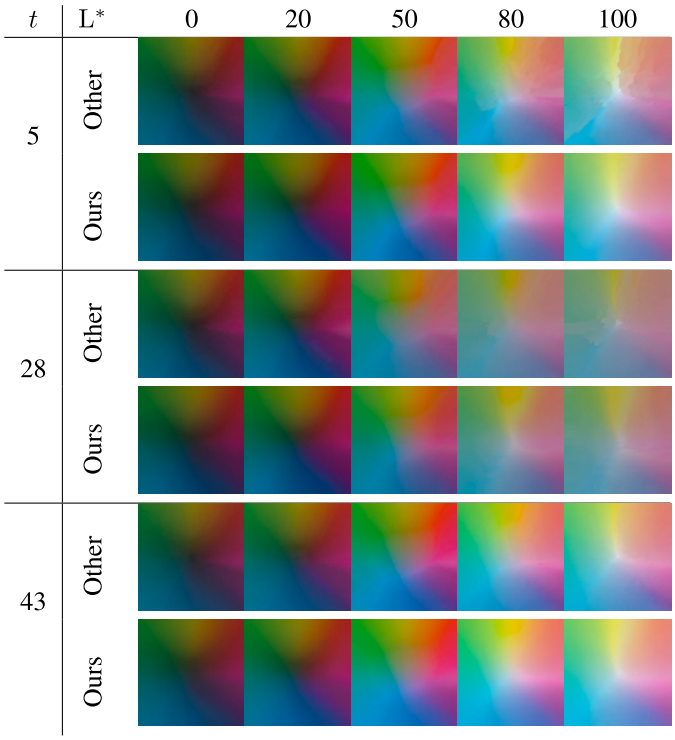

Fig. 13. Transformed images $\mathbf{p}_\gamma(\mathbf{B}(\mathbf{LAB}^t))$ of the Stratasys color and translucency profiles for different lightness L* and translucency levels t created with a proprietary software (top row) and our approach (bottom row). The smoothness of the output is increased especially for bright colors in the translucency level $t = 5$.

Because of the tonal $\mathbf{M}_\Delta$ term the smoothness is also increased in the tonal value space.

B. Translucency

To show that our algorithm can be used to create a joint color and translucency profile we have optimized the profile of a Stratasys J750 Polyjet 3D printer. We compare the output with a color-and-translucency profile that was created with a proprietary software using an algorithm described in [7], where the tonal space is sampled and mapped to select the color that matches the metamer with the most similar translucency. First the color only table is optimized identically as before, then the tables for the subsequent translucency levels are each optimized 3 times with the tonal offset step sizes $\{8, 5, 3, 2, 1, 1\}$ for a total of 18 iterations per level.

Fig. 12 shows the average metric for each L* slice for each translucency level t before and after the optimization.

Compared to the Mimaki printer, the gamut of the Stratasys printer has no sharp edges at the boundary and the input profile does not contain structural artifacts in the color-only table, i.e. for $t = 1$ at the fully opaque $\alpha_1 = 1.0$. Therefore this output could not be improved much by the optimization, but for other translucency levels we can see greater improvements of the metric, especially for bright colors our output is on average better for all t and L*.

The figure also shows the CIEDE2000 average between $\mathcal{R}$ and the mapped colors $\mathbf{p}_\gamma(\mathbf{B}(\mathbf{LAB}^t))$ and $\mathbf{p}_\gamma(\mathbf{B}^*(\mathbf{LAB}^t))$ for each translucency level, with our iCID optimized profile producing a smaller color difference.

Due to the nature of 3D Polyjet printing, where the amount of color material per voxel is limited, adding more transparent material limits the amount of colored inks per volume and effectively reduces the gamut. Since in this case the clear material replaces the white material this results especially in bright colors being out of gamut and consequently a higher metric. Note that due to lateral light transport translucent colors have intrinsically higher reproduction errors than fully transparent colors that were measured on a white background.

Fig. 13 shows a comparison of the transformed output $\mathbf{p}_\gamma(\mathbf{B}(\mathbf{LAB}^t))$ before and after the optimization for some L* lightness and t translucency levels. Visible especially for bright colors, e.g. $L^* = 100$, the output of the unoptimized profile shows strong structural artifacts for $t = 5$ and $t = 28$ that are not present in the output of the optimized profile.

Computing a single iteration step required on average 114 seconds, it is slower than the color-only optimization because of the additional dimension in the look-up-tables. The optimization per translucency level t took on average about 34 minutes using 18 iterations, in total about 24 hours to compute all 42 translucency levels of the color-and-translucency CLUT.

VI. Conclusion and Outlook

We presented an iterative algorithm that optimizes the B2A CLUT defining the backwards transform of an ICC color

profile to improve especially the smoothness but also the color accuracy of the transformation output. It significantly reduces the iCID image difference metric for the evaluated color profiles, resulting in profiles with reduced or removed structural artifacts without sacrificing color accuracy as it also reduces the CIEDE2000 color error to an ideal reference.

The resulting CLUT will reflect all changes introduced by the creation of the references. In particular, if the hue angles are intentionally altered in the input CLUT, the resulting CLUT will reverse these intended changes. The optimization process can arbitrarily alter properties of the profile such as the black generation strategy. Furthermore, gamut clipping transformations might be changed to slight gamut compression to avoid discontinuities.

We have shown that this approach can also be used to create profiles with attributes beyond color, in this case with a transparent clear ink to reproduce translucency. In comparison to an already established algorithm we see significant improvements in the smoothness of the output, allowing the printer to reproduce gradients with higher perceptual similarity.

The brute force approach takes a significant time to compute, especially for color and translucency profiles, even thought most parts can be done in parallel or massively parallel. Since this process is only computed offline once for each profile this is not a problem in practice. Some of the parameters, such as the number of iterations or the used step sizes, are based on empirical observations and might not be optimal w.r.t. convergence or performance.

A. Limitations

It is not possible to create the backwards transform $\mathbf{B}$ of a color profile from scratch just using a forward model, it is necessary to have already a reasonable starting point for the B2A CLUT to compute the references of the optimization.

If the initial profiles backward model's gamut mapping contains lightness inversion artifacts the references will also encode this, we can see this for the Mimaki profile where a very dark cyan material results in darker blue colors than the darkest color of the gray axis. Then the optimization will also produce a backward model with the same lightness inversion. Adjusting the references, either by clipping the L^* value to the darkest color of the gray axis or by using the ideal L^* values in some regions, can reduce this problem but may result in a smaller gamut or undesired color shifts.

Another important requirement for this optimization to optimize color profiles of 3D printers is that the optical printer forward model is accurate and smooth. If the forward model is not smooth the optimization can produce smooth output in the color space that might not be smooth in the tonal space and lead to artifacts that are not visible in the simulation but lead to problems in the halftoning of the printing process. When optimizing color profiles for devices not reliant on halftoning, e.g. RGBW Displays, this can be less of an issue.

For the color and translucency profile the translucency values are only correct along the gray axis and can be slightly off for other colors.

B. Future Work

The use of reference images allows interesting adjustments of the optimization to create profiles that are optimized with specific properties, especially regarding the gamut mapping. For example we can steer the optimization for out of gamut colors to prioritize the lightness reproduction over the hue and chroma, even locally for specific regions of the color space.

Adding more terms to the metric $\mathbf{M}$ or restricting the tonal values $N_\Omega(\mathbf{B}(x))$ considered for optimizing a grid point x based on some secondary criteria could be used to enforce or preserve also other properties of the profile, such as the black generation strategy or total area coverage.

Using a derivative or gradient of the iCID metric would allow to also use other optimization algorithms like gradient descent that might converge faster or find better minima. Future work could also define a stopping criterion which could reduce the number of iterations and therefore the run-time, especially for profiles with attributes beyond color.

Currently the iCID image difference metric is only defined for 2D images, the presented algorithm is not a true 3D optimization but rather a 2.5D approach. Extending the iCID or using a different image difference metric that operates in the 3D space might improve the optimization. Also the iCID is only defined for the CIELAB color space and does not include translucency, extending the metric could further improve the color-and-translucency profile creation.

ACKNOWLEDGMENT

The authors would like to thank Andre Schulz for the CUDA iCID implementation and also would like to thank Alan Brunton as well as the reviewers for their helpful feedback.

REFERENCES

[1] ICC. (2010). *File Format for Color Profiles*. [Online]. Available: http://www.color.org

[2] G. Sharma, *Digital Color Imaging Handbook*, 1st ed. Boca Raton, FL, USA: CRC Press, 2003.

[3] A. Balaji, G. Sharma, M. Q. Shaw, and R. Guay, "Hierarchical compression of color look up tables," in *Proc. Color Imag. Conf.*, vol. 2007. Springfield, VA, USA: Society for Imaging Science and Technology, 2007, pp. 261–266.

[4] Z. Wang, A. Aristova, and J. Y. Hardeberg, "Evaluating the effect of noise on 3D LUT-based color transformations," in *Proc. Conf. Colour Graph., Imag., Vis.* Springfield, VA, USA: Society for Imaging Science and Technology, 2010, pp. 88–93.

[5] K. Falkenstern, N. Bonnier, H. Brettel, M. Pedersen, and F. Viénot, "Using image quality metrics to evaluate an ICC printer profile," in *Proc. Color Imag. Conf.* Springfield, VA, USA: Society for Imaging Science and Technology, 2010, pp. 244–249.

[6] V. Monga and R. Bala, "Algorithms for color look-up-table (LUT) design via joint optimization of node locations and output values," in *Proc. IEEE Int. Conf. Acoust., Speech Signal Process.*, Mar. 2010, pp. 998–1001.

[7] A. Brunton, C. A. Arikan, T. M. Tanksale, and P. Urban, "3D printing spatially varying color and translucency," *ACM Trans. Graph. (TOG)*, vol. 37, no. 4, pp. 1–13, 2018.

[8] P. Urban, T. M. Tanksale, A. Brunton, B. M. Vu, and S. Nakauchi, "Redefining a in RGBA: Towards a standard for graphical 3D printing," *ACM Trans. Graph.*, vol. 38, no. 3, pp. 1–14, Jun. 2019.

[9] M. R. Rosen, E. F. Hattenberger, and N. Ohta, "Spectral redundancy in a six-ink ink jet printer," *J. Imag. Sci. Technol.*, vol. 48, pp. 194–202, May 2004.

[10] P. Zolliker, "Continuity of gamut mapping algorithms," *J. Electron. Imag.*, vol. 15, no. 1, Jan. 2006, Art. no. 013004.

[11] M. Mahy, "Calculation of color gamuts based on the Neugebauer model," *Color Res. Appl.*, vol. 22, no. 6, pp. 365–374, Dec. 1997.
[12] P.-C. Hung, "Colorimetric characterization beyond three colorants," in *Proc. SPIE*, vol. 3963, pp. 196–207, Dec. 1999.
[13] J. Morovic, A. Albarran, J. Arnabat, Y. Richard, and M. Maria, "Accuracy-preserving smoothing of color transformation LUTs," in *Proc. Color Imag. Conf.*, 2008, pp. 243–246.
[14] M. Bhachech, M. Shaw, and J. M. DiCarlo, "Improved color table inversion near the gamut boundary," in *Proc. Color Imag. Conf.*, 2006, pp. 44–49.
[15] J. Preiss, F. Fernandes, and P. Urban, "Color-image quality assessment: From prediction to optimization," *IEEE Trans. Image Process.*, vol. 23, no. 3, pp. 1366–1378, Mar. 2014.
[16] Z. Wang, A. C. Bovik, H. R. Sheikh, and E. P. Simoncelli, "Image quality assessment: From error visibility to structural similarity," *IEEE Trans. Image Process.*, vol. 13, no. 4, pp. 600–612, Apr. 2004.
[17] J. Morovic, *Color Gamut Mapping*. Hoboken, NJ, USA: Wiley, 2008.
[18] J. Morovic, "To develop a universal gamut mapping algorithm," Ph.D. dissertation, Colour Imag. Inst., Univ. Derby, U.K., 1998.
[19] I. Lissner and P. Urban, "Toward a unified color space for perception-based image processing," *IEEE Trans. Image Process.*, vol. 21, no. 3, pp. 1153–1168, Mar. 2012.
[20] M. D. Fairchild, *Color Appearance Models*, 3rd ed. West Sussex, U.K.: Wiley, 2013.
[21] P.-C. Hung and R. S. Berns, "Determination of constant hue loci for a CRT gamut and their predictions using color appearance spaces," *Color Res. Appl.*, vol. 20, no. 5, pp. 285–295, Oct. 1995.
[22] L.-Y. Wei, "Parallel Poisson disk sampling," *ACM Trans. Graph.*, vol. 27, no. 3, pp. 1–9, Aug. 2008, doi: 10.1145/1360612.1360619.
[23] B. M. Vu, T. M. Tanksale, P. Urban, and S. Nakauchi, "Visual perception of 3D printed translucent objects," in *Proc. 24th Color Imag. Conf.*, San Diego, CA, USA, 2016, pp. 94–99.
[24] D. Chen and P. Urban, "Deep learning models for optically characterizing 3D printers," *Opt. Exp.*, vol. 29, no. 2, pp. 615–631, 2021.
[25] M. M. Saguer. (2021). *Little CMS 2*. [Online]. Available: https://www.littlecms.com/color-engine/

Johann Reinhard received the B.Sc. degree in computer science and the M.Sc. degree in visual computing from Technical University Darmstadt, Germany, in 2017 and 2019, respectively. Since 2019, he has been a Researcher with the Competence Center 3D Printing Technology, Fraunhofer Institute for Computer Graphics Research, Darmstadt, and works on the graphical 3D printer driver "Cuttlefish" and the data-driven design tool "Cuttlefish:Eye." His research interests include 3D printing, image processing, and machine learning.

Philipp Urban received the M.S. degree in mathematics from the University of Hamburg, Germany, in 1999, and the Ph.D. degree from the Hamburg University of Technology in 2005. From 2006 to 2008, he was a Visiting Scientist with the Munsell Color Science Laboratory, Center for Imaging Science, Rochester Institute of Technology, Rochester, NY, USA, and headed afterwards the Color Research Group, Institute of Printing Science and Technology, Technische Universität Darmstadt, Darmstadt, Germany. Since 2013, he has been the Head of the Competence Center 3D Printing Technology, Fraunhofer Institute for Computer Graphics Research IGD, Darmstadt, where he and his team develop the graphical 3D printer driver "Cuttlefish" and the data-driven design software "Cuttlefish:Eye." He is an Adjunct Professor with the Norwegian Colour and Visual Computing Laboratory, Norwegian University of Science and Technology (NTNU), Norway. His research interests include 3D printing, spectral imaging, image quality, and material appearance reproduction.